Nanoscale

Accepted Manuscript

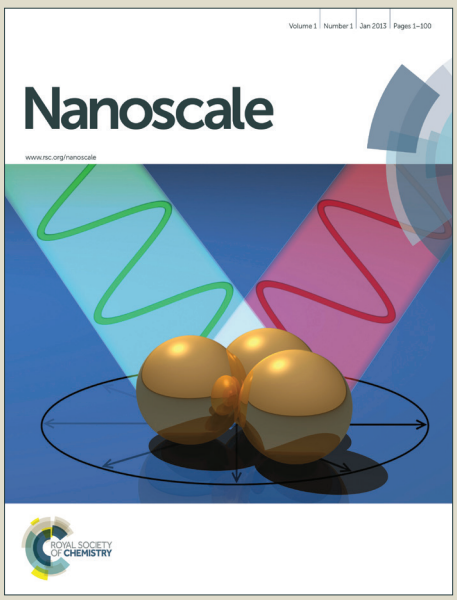

ROYAL SOCIETY OF CHEMISTRY

www.rsc.org/nanoscale

Cite this: DOI: 10.1039/c0xx00000x

www.rsc.org/xxxxxx

COMMUNICATION

Real space probe of short-range interaction between Cr in a ferromagnetic semiconductor ZnCrTe

Ken Kanazawa, Taku Nishimura, Shoji Yoshida, Hidemi Shigekawa and Shinji Kuroda

Received (in XXX, XXX) Xth XXXXXXXXX 20XX, Accepted Xth XXXXXXXXX 20XX

DOI: 10.1039/b000000x

The short-range interaction between Cr atoms was directly examined by scanning tunneling microscopy measurements on a $Zn_{0.95}Cr_{0.05}Te$. Our measurements revealed that a Cr atom formed a localized state within the bandgap of ZnTe and this state was broadened for a pair of Cr atoms within a distance of ~1 nm.

In the past few decades, so-called "spintronics", which utilizes both the charge and spin characteristics of carriers, has been attracting considerable attention. Diluted magnetic semiconductors (DMSs), in which doped magnetic atoms partially substitute the atomic sites in a host semiconductor, have been energetically studied because of their high potential for advancing future semiconductor-based spintronic devices [1]. For practical applications, the development of ferromagnetic DMSs with a higher Curie temperature (T_c) than room temperature (RT) is a key factor. Although the realization of ferromagnetism with T_c higher than RT has been claimed for various DMSs, contradictory results have also been reported despite the fact that the same DMS materials were analyzed. A possible reason for this is that the growth of DMSs is very sensitive to the environmental conditions during growth; a small difference in the growth conditions induces the formation of a compositional fluctuation or a different structural phase, which may give an appearance of ferromagnetism of the synthesized crystals. In order to determine the intrinsic magnetic properties of DMSs studied, it is essential to examine crystals confirmed to be of the pure diluted phase in which the magnetic impurities are distributed randomly on the substitutional sites of the host crystal. In addition, microscopic analysis of the electronic states of magnetic impurities, such as spatial distribution and local density of states, is indispensable for the understanding of the interaction between magnetic impurities and the mechanism of ferromagnetism.

Cr-doped ZnTe is one of the most promising materials for future semiconductor-spintronic applications. Intrinsic RT ferromagnetism has been observed for $Zn_{1-x}Cr_xTe$ ($x \approx 0.2$)[2]. Furthermore, the magnetic properties of (Zn,Cr)Te can be controlled by co-doping carrier dopants [3,4]. In particular, by doping iodine atoms as donors, even when the Cr composition is much smaller ($x \approx 0.05$), a high T_c (~RT) was observed, which was considered to be due to the formation of local Cr-rich regions in which Cr atoms substitute the Zn site in a high concentration [3]. This result is interpreted as a result of the short-range character of the ferromagnetic interaction between Cr, which is considered to act effectively between Cr atoms located within a short distance in the Cr-rich regions. This is different from the case of (Ga,Mn)As, whose ferromagnetic mechanism has been regarded as carrier-mediated interaction [5]. Therefore, microscopic analysis of the characteristics of the Cr-Cr interaction in ZnTe crystal is essential. A double-exchange or superexchange interaction was theoretically proposed as a possible mechanism to explain the magnetism in (Zn,Cr)Te [6,7], which, however, has not yet been clarified experimentally. Here, we present the results obtained in a scanning tunneling microscopy/spectroscopy (STM/STS) study on (Zn,Cr)Te. The short-range interaction between Cr atoms, which is considered to characterize the magnetism in (Zn,Cr)Te, was directly examined in real space for the first time.

Figure 1 (a) shows a typical STM topographic image of a ($Zn_{0.95}$, $Cr_{0.05}$)Te /ZnTe buffer/p-ZnTe cross-sectional surface (see method). The interface between the substrate and the MBE layer was clearly distinguished. Figures 1(b) and 1(c) are magnified STM images of the (Zn,Cr)Te and p-ZnTe substrate regions, respectively. In addition to the rows of Te atoms along the [110] direction, several line defects along the [110] direction can be

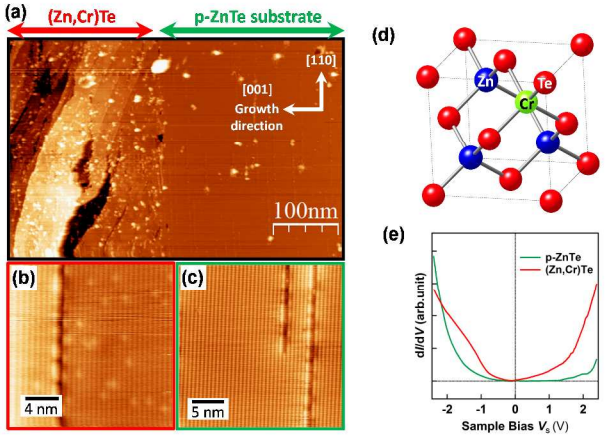

Fig.1 STM/STS measurements of (Zn,Cr)Te/p-ZnTe. (a) Cross-sectional STM topographic image of (Zn,Cr)Te/p-ZnTe multilayered structure (V_s = +5.0 V, I = 20 pA). (b) and (c) Magnified STM images of the (Zn,Cr)Te layer (V_s = -2.0 V, I = 40 pA) and the p-ZnTe substrate (V_s = -1.5 V, I = 60 pA), respectively. (d) Schematic view of (Zn,Cr)Te unit cell including a substitutional Cr atom. (e) dI/dV-V spectra averaged over the (Zn,Cr)Te and ZnTe areas shown in (a).

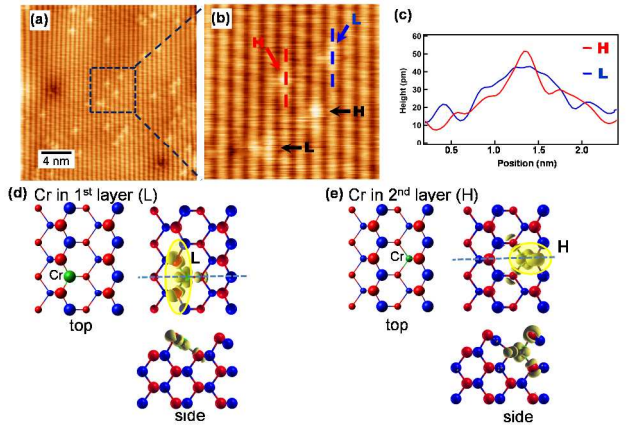

Fig.2 STM observation of Cr atoms on a (Zn,Cr)Te surface. (a) High resolution STM image of Cr dopant atoms on a (Zn,Cr)Te(110) surface (V_s = -2.0 V, I = 10 pA). (b) Magnified image of the area indicated by the dotted square in (a). H and L indicate the two types of image with two different heights. (c) Cross sections obtained along the two dashed lines in (b). (d) and (e) results of the DFT calculations for the Cr atoms located in the first and second (110) atomic layers, respectively. Spatial distributions are the LDOS integrated over E_F-0.1 eV < E < E_F (E_F: Fermi energy). The side-view images below represent cross-sectional drawings along the dashed lines in the respective top-view images.

seen, which correspond to the monoatomic-wide rows of vacancies generally observed on a cleaved ZnTe(110) surface [8]. From the asymmetry in the brightness on the both sides of the line defects, the distinction of the in-plane crystallographic orientations between [110] and [-110] was determined, as shown in Fig. 1(a) [9]. In addition to such intrinsic atomic structures on the cleaved ZnTe surface, the STM image in Fig. 1(b) shows a number of atomic-scale bright structures in the terrace area, which are attributed to doped Cr atoms in the surface region. To investigate the effect of Cr atoms, STS measurement was carried out. As shown in Fig. 1(e), the dI/dV-V curves averaged over the (Zn,Cr)Te and ZnTe areas in Fig. 1(a) are different from each other. The dI/dV obtained over the (Zn,Cr)Te area shows the existence of in-gap states. From an early theoretical study of the electronic configuration of (Zn,Cr)Te [6], these states are considered to be the localized state of Cr 3d electrons.

Figures 2(a) and 2(b) show a high-resolution STM image of the (Zn,Cr)Te layer and its magnification, respectively. The cross sections along the two lines in Fig. 2(b) are shown in Fig. 2(c). The in-plane dimension of the Cr image is about 1 nm, considerably smaller than the size of Mn and Fe atoms observed in a GaAs matrix beneath the surface at a similar negative bias voltage [10], i.e., the acceptor state images of ionized A^- and neutral A^0 states for Mn and Fe, respectively. In general, a shallow acceptor or donor impurity in a host semiconductor is imaged as a relatively large structure because of its disperse electronic charge distribution. In contrast, since Cr^{2+} state in (Zn,Cr)Te is deep (~1.3 eV from the valence band top), it remains in the form of Cr^{2+} without generating holes in the host ZnTe even under a tip-induced band bending at the bias voltage of ~ -2.0 V. Therefore, the observed small size of the Cr images is also consistent with a deep energy position within the band gap of Cr atoms substituting the Zn site of the host crystal. The Cr images were classified into two types with two different heights, as indicated by H (high) and L (low) in Fig. 2(b). To clarify the two types of structure, we carried out a simple density functional theory (DFT) calculation using the spin-polarized Perdew-Burke-Ernzerhof generalized gradient approximation (PBE-GGA) with the ABINIT code[11] with plane-wave-based norm-conserving pseudopotentials (see method).

Figures 2(d) and 2(e) show the DFT results of local density of states (LDOS) integrated over E_F-0.1 eV < E < E_F (E_F: Fermi energy) for the Cr atoms located in the first and second (110) atomic layers, respectively. A large LDOS area, which is bright in the STM image [12], exists near the topmost Te atoms neighboring the Cr for the both structures. The anisotropic shape indicates that the Cr-related states, which contributed to the STM image, were hybridized with the states of the nearby Te atoms. The spatial distribution of the LDOS formed by the Cr in the second layer is more localized and higher than that formed by the Cr in the first layer, and these two states are considered to correspond to the H and L states observed by STM, respectively. The Cr atoms in deeper sites were not observed unlike the case of the Mn atoms in a GaAs matrix. This is considered to be due to the small spatial extent of the Cr states discussed above.

Next, to investigate the Cr-related electronic states in more detail, we performed STM/STS analyses at a single-atomic level. Figure 3(a) shows an STM image of a (Zn,Cr)Te region. Figures 3(b) to 3(d) respectively show magnified images of the three regions indicated by A, B and C in Fig. 3(a), with circular low-pass filtering, whose radius is insignificantly smaller than the distance between the central point and the spot generated from [110] atomic rows, carried out in order to enhance the contrast of local structures and make the position of them clear. The Cr images labeled #1, 2, 4, 5 and 6 were classified into the two types indicated in Fig. 2, H and L, by measuring their heights and positions with respect to the surface lattice of the topmost Te atoms indicated by the dashed lines, and the schematic structures illustrating their occupying sites in (Zn,Cr)Te are also shown. The additional two images, L in A and H in C, were determined in the similar way.

The image labeled by #3 was brighter (about 0.3 Å higher) and more elongated along the [110] direction than the Cr atoms in the H state. In order to analyze the atomic arrangement, we performed DFT calculation for the <110> Cr-Cr pair located in the first (110) atomic layers. Figure 4(a) shows the magnification of the STM image labeled #3 in Fig. 3(d), in which lattice mesh and Zn, Te and Cr atoms are shown together. The results of the calculations obtained for V_s= -0.1V (E_F-0.1 eV < E < E_F) and V_s= +0.5V (E_F < E < E_F+0.5 eV) are shown in Figs. 4(c) and 4(d), respectively. Due to the effect of overlap of impurity states of the two Cr atoms, the topmost Te atom, which is located at the center between the Cr atoms, has different states from those of the other topmost Te atoms neighboring Cr. When we compare the calculated distribution of LDOS for these atoms in the occupied state (c) and the unoccupied state (d), the overall features are not different with each other, but the protrusion of 0.35 Å at the position of the central Te atom relative to the other neighboring atoms, which should be in a similar state to the "L", in (d) suggests that the observed STM image for Cr #3 would be closer to the distribution of the unoccupied state (d). These results indicate that despite that the STM image is obtained at a negative bias voltage, unoccupied states are included. This is considered to

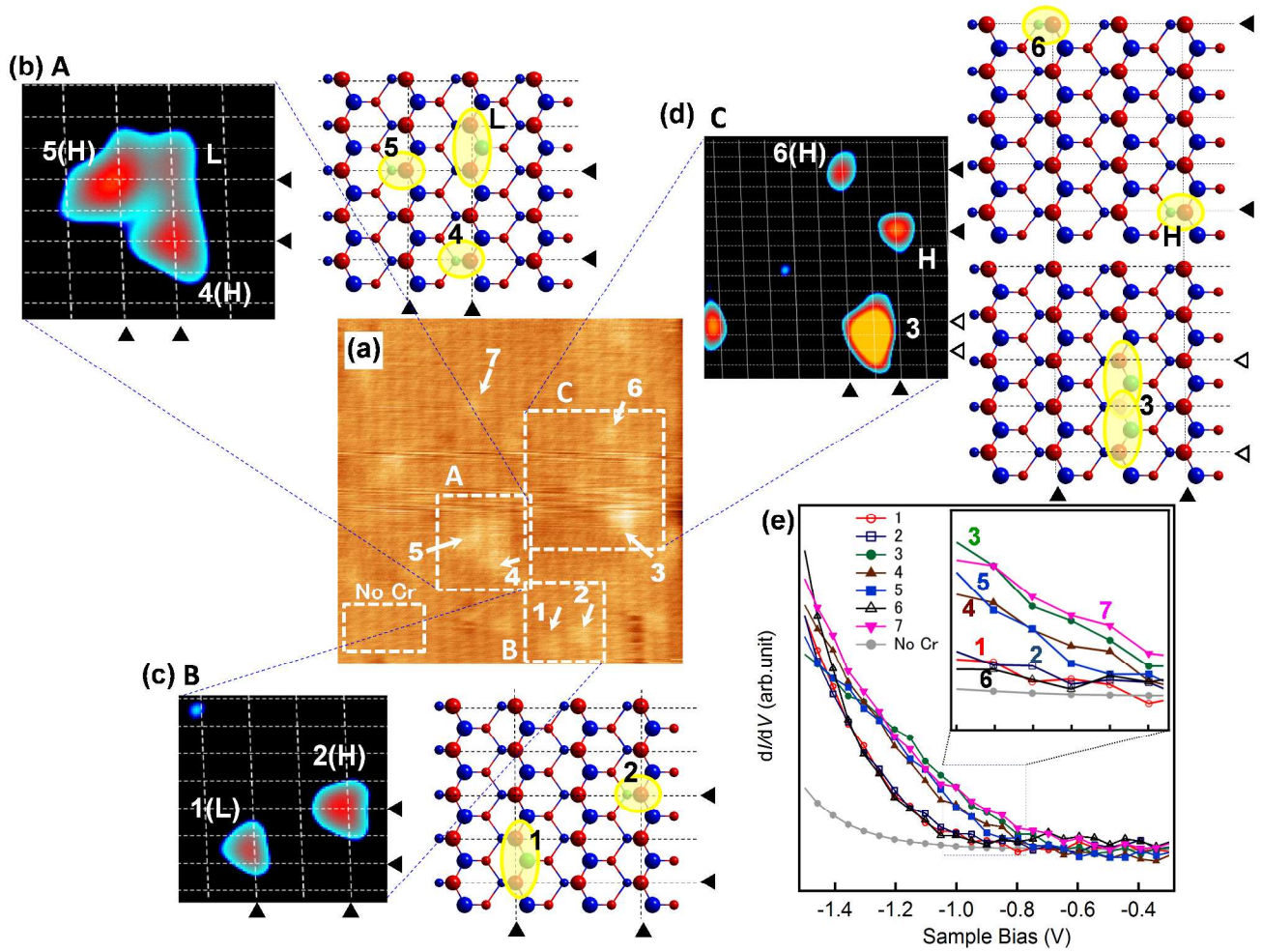

Fig.3 STM/STS analyses of Cr-Cr interaction. (a) STM image of (Zn,Cr)Te area (V_s = -2.0V, I = 20 pA). (b), (c) and (d) Left: magnified images of the square areas indicated by A, B and C in (a), respectively. Low-pass filtering was carried out to enhance the local electronic structures. Right: Schematic structures of the atomic configurations of the STM images on the left. (e) dI/dV-V spectra measured above the Cr atoms labeled #1 to #7 and on the area of ZnTe without Cr in the bottom-left square shown in (a). The inset is a magnification of the dI/dV-V curves in the square region.

be due to the influence of the tip induced band bending (TIBB). In order to estimate the effect of the TIBB actually, we performed light-modulated scanning tunneling spectroscopy (LM-STS) [13] with a semiconductor laser, whose wavelength and light-intensity are 400 nm and 5 mW, respectively. The LM-STS result was shown in Fig.4(d). With the chopped laser illumination, the two virtual I–V curves, which correspond to those under dark (I_{off} : blue) and illuminated (I_{on} : red) conditions, can be simultaneously obtained. The spectrum of the surface photo voltage (SPV), which provides information about the polarity and magnitude of the surface band bending under the dark condition, is obtained by calculating the lateral shift of the two I–V curves with respect to the bias voltage for the I–V curve under the dark condition (green circles). The SPV value of about -0.4 V at V_s = 0 V is almost consistent with the above discussion, in which the STM image may reflects the unoccupied surface states in the range of $E_F < E < E_F$+0.5 eV despite the observation at negative V_s. For the respective Cr pairs shown in Fig.3, the distances and the directional relations between the two Cr atoms are summarized in Table 1.

To obtain a deeper understanding of the interaction between Cr atoms, analysis of the electronic state of Cr 3d electrons in the atomic scale is essential. In fact, as shown in Fig. 1(e), the localized state of Cr 3d electrons appeared as in-gap states in the STS spectrum. To examine the interactions between Cr atoms, we carried out dI/dV-V measurement. Figure 3(e) shows the dI/dV-V spectra measured above the Cr atoms labeled #1 to #7 and on the area of ZnTe without Cr in the bottom-left square shown in Fig. 3(a). The inset of Fig. 3(e) is a magnification of the dI/dV-V curves in the range of bias voltage -1.0 V < V_s < -0.8 V, in which the dI/dV-V curves rise from zero value.The spectrum obtained over the area of ZnTe without Cr is similar to that obtained for the p-type substrate shown in Fig. 1(e). The dI/dV spectra measured above the Cr atoms in the atomic scale clearly exhibited a larger DOS than that obtained over the area of ZnTe without Cr, similarly to the results shown in Fig. 1(e). However, the spectra were divided into two types with different behaviors in the range of bias voltage -1.4V < V_s < -0.8 V; the dI/dV-V curves measured above Cr #3,4,5,7 rise at a relatively smaller bias voltage at around -0.8V and has larger values in the negative

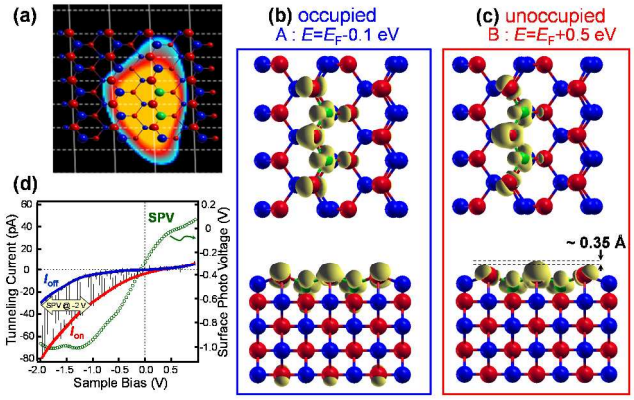

Fig4 STM image and DFT calculations for the structure labeled 3 in Fig. 3. (a) Magnification of the low-pass filtered image of label 3 shown in Fig. 3(d) and schematic of its structural model. Results of DFT calculations of local density of states (LDOS) integrated over (b) E_F-0.1 eV < E < E_F and (c) E_F < E < E_F+0.5 eV. (d) Typical LM-STS spectra obtained on (Zn,Cr)Te measured with a semiconductor laser (λ = 400 nm, Light-intensity = 5 mW). For example, the yellow arrow indicates the magnitude of the surface photo voltage at V_s=-2.0 V

bias region -1.4V < V_s < -0.8V than those measured above Cr #1, 2, 6. The bias voltage at which the dI/dV curve starts to rise from zero for the respective Cr atoms is also listed in Table 1. This difference in the dI/dV-V curves shows a clear correlation with the distance to the neighboring Cr atom shown in Table 1; the value of dI/dV in this range is large for a Cr atom with its neighbor within 1.1 nm while the value is small for a Cr atom with its neighbor beyond 1.1 nm. Therefore, the larger values of dI/dV of Cr #3,4,5,7 are interpreted as a result of broadening of the Cr localized state due to the interaction with the neighboring Cr atom. The observation of this broadening only for Cr pairs with a short distance less than 1nm indicates the short-range character of the interaction between Cr.

The spectra measured above Cr #1,2,6, which are considered to be unaffected by the interaction, are very similar to each other, regardless of whether the Cr atom was located in the first or second layer from the surface. On the other hand, a slight difference can be seen among the spectra measured above Cr #3,4,5,7. The spectra of Cr #3,7 rise at slightly smaller bias voltages than those of Cr #4,5, as shown in Fig. 3(e). Since the distance between Cr atoms in Cr #3, which consists of the nearest-neighbor pair, is much shorter than Cr #4,5, the difference in the spectra is considered to reflect the strength of the interaction; the Cr localized state is much more broadened due to a stronger interaction between Cr atoms within a shorter distance. The spectrum of Cr #7 is almost similar to that of Cr #3, in spite of the isolated appearance in the observed STM image. A possible explanation for this apparent contradictory observation is that there is another Cr atom in the nearest neighbor site underneath the observed Cr atom.

To examine the Cr-Cr distance dependence of the spectra in more detail, we calculated the DOS for various atomic arrangements of Cr-Cr pairs in the host ZnTe crystal using GGA-PBE. As a host semiconductor matrix, we used a $2 \times 2 \times 2$ supercell of the ZnTe crystal structure. One (0) or two (0 and one of 1-5) of the 32 Zn sites in the supercell shown in Fig. 5(a) were replaced by one or two Cr atoms, and the energy distribution of the spin-dependent DOS was calculated for each structure.

Table 1 Summary of the configurations of Cr atoms. The value of V_s at which dI/dV-V curves in Fig.3 rise from zero value are also listed.

Cr-Cr pair	Direction	Distance (nm)	V_s at dI/dV rise in Fig.3(e) (V)
3	<110>	0.43	-0.7
4-L	<123>	1.14	
5-L	<013>	0.96	-0.8
4-5	<111>	1.06	
1-2	<123>	1.14	-0.9
6-H	<111>	2.11	-0.9

Figures 5(b) and 5(c) respectively show the results obtained for undoped ZnTe and ZnTe doped with a single Cr. Spin-polarized states were formed in the energy gap region of the host ZnTe by the doped Cr atom. The calculated DOS was basically similar to the earlier theoretical studies [6,7], though the in-gap states were located at a shallower energy level relative to the host valance band than the experimental results of earlier photo-EPR and optical absorption measurements [14].

According to the earlier study [6], the observed in-gap states consist mainly of t^a states, which originate from Cr 3d-electrons. The five energy levels are degenerate in a free atomic state, however, when a Cr atom substitutes the Zn site to form a tetrahedral coordination with the neighboring Te atoms, these energy levels are split into triply-degenerate dε and doubly-degenerate dγ states by the crystal field. Moreover, because the electronic orbitals of the dε states are strongly hybridized with the valence electrons of Te atoms, bonding states t^b and anti-bonding states t^a are formed in the valence band and in the ZnTe band gap,respectively. Since the hybridization between the dγ states and the host valence states is weak, they form non-bonding states, e, at a lower energy position than that of t^a. The Cr 3d-electrons and Te p-electrons occupy the exchange-split hybridized states until the t^a level with the spin-up state, at which the Fermi level E_F is located. Therefore, the electronic states near the Fermi energy are dominated by t^a impurity states. The V_s=0 in a STS spectrum generally corresponds to the E_F of the sample surface. However, in our STS measurement, dI/dV-V curves start to deviate from zero at V_s ~-0.9 V for the isolated Cr atom (Fig. 3(e)), not at V_s=0. In addition, the result of calculation in Fig. 5(d) indicates that the DOS starts to rise from zero at a position ~0.5 eV above E_F. These results, therefore, suggest a difference of ~1 eV between the value of V_s in the observed STS spectra and the value of E_F in the calculated DOS. A possible reason for the difference is the influence of band bending of ~1eV at V_s ~-0.9 V. This is in good agreement with the result of the LM-STS measurement as shown in Fig. 4(d) and the fact that the STM image of the label #3 includes the unoccupied states despite the negative bias voltage used in measurement as pointed out before. The band bending is mainly caused by the difference of workfunctions between W-tip and (Zn,Cr)Te [15].

When a pair of Cr atoms is located within a short distance, the half-filled t^a states interact with each other due to the ferromagnetic coupling (double exchange mechanism) and the electronic states are considered to be broadened. Figure 5(d) shows the calculated DOSs for Cr pairs with different arrangement, where the configurational dependence of the spectra can be clearly shown. In particular, a nearest-neighbor Cr pair in the [110] direction exhibited the electronic state with the broadest energy dispersion and the strongest exchange ferromagnetic

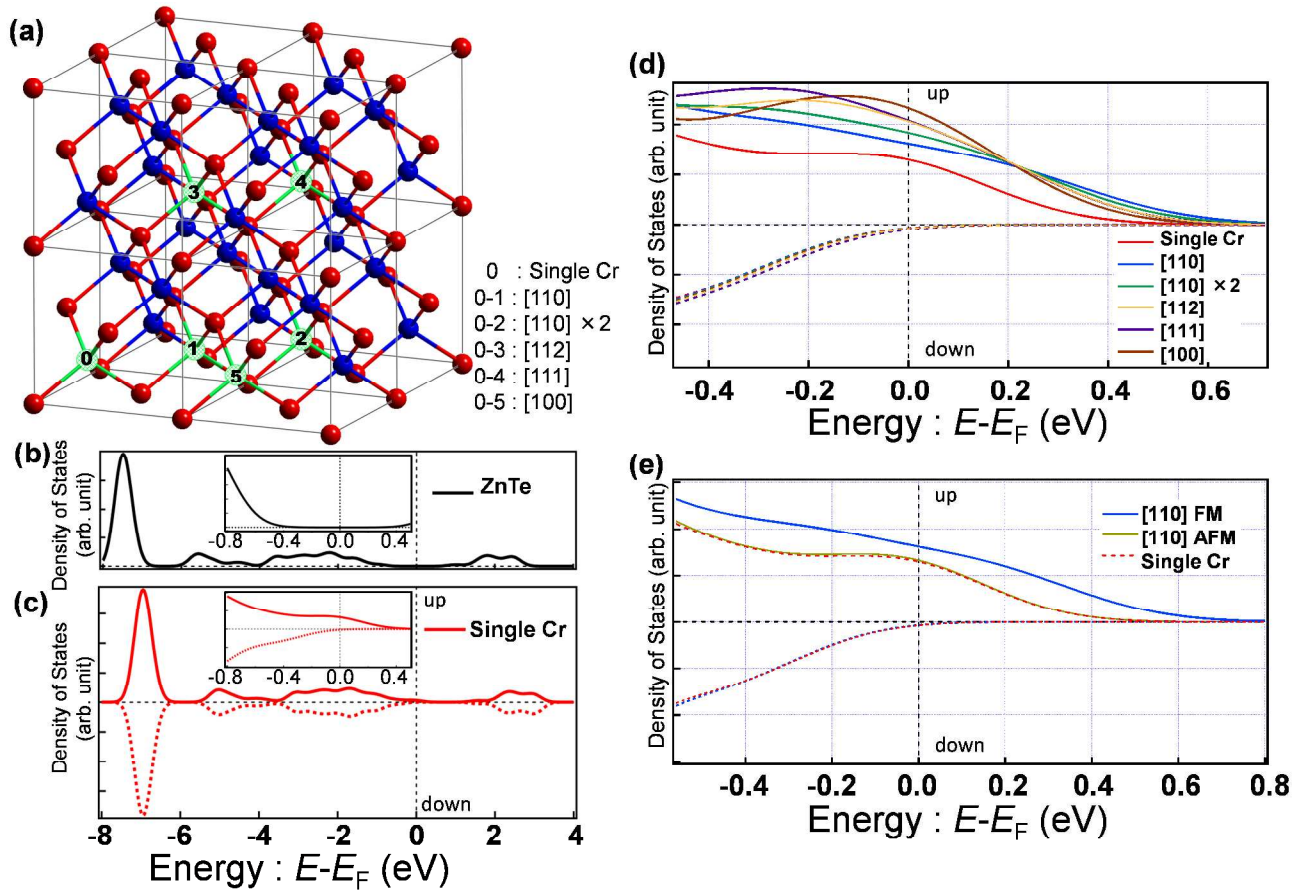

Fig. 5 DFT calculations of DOSs for ZnTe and (Zn,Cr)Te structures. (a) Schematic structure of 2×2×2 supercell used for calculation. One (0) Zn or two (0 and one of 1-5) Zn atoms of the 32 Zn sites were replaced by one/two Cr atoms in the calculations. (b) DOS obtained for undoped ZnTe. (c) DOS obtained for the ZnTe doped with a single Cr atom at the site labeled 0. Up and down indicate spin directions. (d) DOSs calculated for various Cr-Cr configurations indicated by different colored lines. (e) DOSs calculated for the Cr-Cr structures with ferromagnetic and antiferromagnetic spin orientations.

interaction estimated from the total energy difference between antiferromagnetic (AFM) and ferromagnetic (FM) states (E_{FM}-E_{AFM}), as shown in Table 2. These results are also in good agreement with the experimentally obtained spectra shown in Fig. 3(e). Finally as shown in Fig. 5(e), for an antiferromagnetic Cr-Cr pair in the [110] direction, the calculated DOS is almost the same as that of a single Cr atom. Namely, broadening occurs only when the alignment of Cr spins is ferromagnetic, as expected. Here, we have to refer to the superexchange interaction as another possible mechanism of the ferromagnetism with short-range character in this system. Generally, the superexchange interaction should work between two Cr atoms in the nearest neighboring arrangement through a Te atom located between the two Cr atoms. However, the broadening of the Cr impurity state due to the ferromagnetic interaction was observed for the Cr pairs whose interval is farther than that of the nearest neighboring arrangement. This result suggests that the double exchange interaction is suitable to explain the ferromagnetic mechanism.

As a preceding STM study on the interaction between magnetic impurities in a DMS, Kitchen *et al*. observed ferromagnetic interaction between Mn atoms in (Ga,Mn)As [16]. They observed that the in-gap conductance peak in the STS spectra, which originates from the electron tunneling into the empty hole state of

Table2 Summary of theoretical calculations of total energy difference between antiferromagnetic (AFM) and ferromagnetic (FM) states (E_{FM}-E_{AFM}).

Cr-Cr pair	E_{FM} - E_{AFM} (eV)
<110>	-0.192
<110>×2	-0.100
<112>	-0.041
<111>	-0.022
<001>	-0.008

Mn^{2+} ions, split into the bonding and anti-bonding states for a Mn pair due to the interaction between Mn. They found that the strength of the interaction, which was evaluated from the splitting energy of the conductance peaks, depends strongly on the distance and directional relation between Mn atoms; the interaction was the strongest for the nearest neighboring pair along the <110> direction, highly anisotropic, and almost disappeared for pairs beyond the six nearest neighbor. These observed features of the Mn-Mn interaction cannot be explained by the model of the carrier-mediated mechanism; the interaction mediated by free holes should be isotropic and range over relatively long distance. Alternatively, the p-d hopping model

was proposed as a possible ferromagnetic interaction [17]. On the other hand, in the present study on (Zn,Cr)Te, we observed the broadening of the Cr impurity state due to the ferromagnetic interaction between Cr and found that the interaction depends strongly on the distance between Cr atoms, which is quite similar to the interaction of Mn-Mn pairs reported in Ref.[16]. This similarity suggests that the fundamental origin of ferromagnetism in these DMS can be based on a similar short-range interaction directly working between 3d electrons of transition-metal atoms hybridized with valence p electrons of the host anions. This description may give a general understanding of ferromagnetic DMSs.

It should be pointed out that the ferromagnetic interaction appears as a different way between (Zn,Cr)Te and (Ga,Mn)As in the STS measurements; the broadening of the Cr state in (Zn,Cr)Te in contrast to the splitting of the Mn state in (Ga,Mn)As. This difference may reflect the difference in the relative energy position of the magnetic impurity to the valence band of the host semiconductor and in the number of 3d electrons. In the case of (Zn,Cr)Te, the Cr state appears as a continuum state extended from the top of the valence band, which was observed as a conductance tail in the negative bias region in the STS spectra due to a process of the electron tunneling from the occupied state. On the other hand, in (Ga,Mn)As, the Mn hole state was observed as an independent conductance peak in the positive bias region in the STS spectra due to a process of the electron tunneling into the empty state. However, in order to clarify the issue, we need further systematic study. Furthermore, here, the range of the ferromagnetic interaction observed in this study, which works within the distance of ~1.1 nm, has to be compared to the spatial dimension of the ferromagnetic domain of ~ 4 nm measured by D. Soundararajan *et al.* with magnetic force microscopy (MFM) for a $Zn_{0.95}Cr_{0.05}Te$ film grown on a glass substrate[18]. Generally, a dimension of a ferromagnetic domain should be larger than the distance within which a ferromagnetic interaction works between two magnetic dopant atoms. The magnitude relation of these two values in this (Zn,Cr)Te system is consistent with the generality. Furthermore, since a distance between Cr atoms in a ferromagnetic domain should be smaller than 1.1 nm, the local Cr concentration in the magnetic domain observed in the latter MFM study is larger than the average concentration 5 %.

Conclusions

In summary, we have investigated local electronic states of Cr atoms in a diluted magnetic semiconductor (Zn,Cr)Te by cross-sectional STM and STS measurements. We successfully observed single Cr atoms substituting Zn-sites located in the first and second layers from the surface and their impurity states at an energy position located within the band-gap of the host ZnTe. By comparing with the observed STS spectra for Cr pairs with the result of theoretical calculations, we concluded that the impurity state is broadened for a pair of Cr atoms with distance shorter than 1.1 nm due to ferromagnetic interaction, which is in good agreement with a short-range character of ferromagnetic mechanism based on double exchange interaction proposed for this system. These findings are important for the understanding of the origin of magnetic interaction in DMSs. They may also provide helpful information for realization of high-temperature ferromagnetism by using proper bottom-up approach to control the arrangement of magnetic atoms such as atom manipulation by scanning probe microscopy or site selective growth by MBE.

Acknowledgements

Support from Japan Society for the Promotion of Science in the form of Grants-in-Aid for Scientific Research is acknowledged.

Notes and references

Faculty of Pure and Applied Sciences, University of Tsukuba, Tsukuba 305-8573, Japan Fax: +81 29 853 5102; Tel: +81 29 853 5102; E-mail: kanazawa@ims.tsukuba.ac.jp

‡ Methods

A sample with a multi-layered structure was fabricated by molecular beam epitaxy (MBE); a buffer undoped ZnTe layer (thickness ~10 nm) and a ($Zn_{0.95}$, $Cr_{0.05}$)Te (~250 nm) layer were successively grown on a p-type ZnTe (001) substrate (P-doped, 1×10^{18} cm^{-3}). The growth rate was fixed at ~ 1 Å/s with the substrate temperature maintained at 573 K; under these growth conditions, most of the Cr atoms randomly occupy Zn sites in the host ZnTe crystal [3]. During the growth process, the surface was monitored in situ by reflection high-energy electron diffraction (RHEED). A clean cross-sectional (110) surface was obtained by cleaving the sample. All STM/STS measurements were performed with an Omicron low-temperature (LT) scanning tunneling microscope under ultrahigh-vacuum conditions (< 10^{-8} Pa) at 77 K (Fig.1) and 8K (Fig.2 and 3) using an electrochemically sharpened W tip (ϕ= 0.3 mm).

To calculate the electronic states in the surface region, we constructed super cells with slab models consisting of five ZnTe(110) atomic layers and a vacuum region also with a thickness of five atomic layers. The atoms in the topmost layer were displaced from the positions of the ideal (110) surface following the surface reconstruction reported by Meyer *et al.* [19]. On the other hand, to model the in-plane periodicity, we used 3×2 super cells for the [110] and [100] directions. Here, each Zn atom in the slab model was replaced by a Cr atom. Since the STM tunneling current should reflect the LDOS near the Fermi energy (E_F) of the surface region at the STM tip position, we calculated the electronic states around E_F. The plane-wave cutoff energy for all calculations was 60 Ry. And we used 2×2×1 Monkhorst-Pack k-point grids to sample the Brillouin zone. Figures 2(d) and 2(e) show the calculated spatial distributions of the LDOS integrated over the energy region of E_F - 0.1 eV < E < E_F (E_F : Fermi energy) for the structures with a Cr atom located in the first and second layers, respectively. The obtained LDOS is highly concentrated near the Cr atom and spreads from the Cr atom toward the nearest Te atoms. In addition, the LDOS between the Cr atom and a neighboring Te atom is relatively small. These results indicate that the electronic states in this energy region can be mainly attributed to the t^a state.

On the other hand, to calculate the DOS of Cr-Cr pairs in the 2×2×2 supercell of the ZnTe crystal structure as shown in Fig.5, we used 2×2×2 Monkhorst-Pack k-point grids.

1 D. Nikonov and G. Bourianoff, *J. Supercond. Novel Magn.,* 2008, **21**, 479; C.Liu, F.Yun and H.C.Morkoc, *J.Mater.Sci.:Mater. Electron.*, 2005, **16**, 555; S. A. Chamber, *Surf. Sci. Rep.*, 2006, **61**, 345; A. Bonanni, T.Dietl, *Chem. Soc. Rev.,* 2010, **39**, 528; T.Dietl, *Nat. Mater.,* 2010, **9**, 965.

2 H. Saito *et al.*, *Phys. Rev. Lett.*, 2003, **90**, 207202.

3 S. Kuroda, N. Nishizawa, K. Takita, M. Mitome, Y. Bando, K. Osuch and T. Dietl, *Nat. Mater.*, 2007, **6**, 440.

4 N. Ozaki, N. Nishizawa, S. Marcet, S. Kuroda, O. Eryu and K. Takita, *Phys. Rev. Lett.*, 2006, **97**, 037201.; N. Ozaki, I. Okabayashi, T. Kumekawa, N. Nishizawa, S. Marcet, S. Kuroda, and K. Takita, *Appl. Phys. Lett.*, 2005, **87**, 192116.

5 H. Ohno, *Science*, 1998, **281**, 951.

6 K. Sato and H. Katayama-Yoshida, *Semicond. Sci. Technol.*, 2002, **17**, 367.

7 T. Fukushima, K. Sato, H. Katayama-Yoshida, and P. H. Dederichs, *Jpn. J. Appl. Phys.*, 2004, **43** L1416; H. Katayama-Yoshida, K. Sato, T. Fukushima, M. Toyoda, H. Kizaki, V. A. Dinh and P. H. Dederichs, *phys. Stat. sol. (a)*, 2007, **204**, 15.

8 A. Wierts, J. M. Ulloa, C. Çelebi, P. M. Koenraad, H. Boukari, L. Maingault, R. André and H. Mariette, *Applied Physics Letters*, 2007, **91**, 161907.

9 C. Çelebi,O. Arı,and R. T. Senger, *Phys. Rev. B,* 2013, **87**, 085308.

10 A. M. Yakunin *et al., Phys. Rev. Lett.,* 2004, **92**, 216806.; J. Bocquel, V. R. Kortan, C. Şahin, R. P. Campion, B. L. Gallagher, M. E. Flatté, and P. M. Koenraad, *Phys. Rev. B*, 2013, **87**, 075421.

11 X. Gonze *et al., Computat. Mater. Sci*. 2002, **25,** 478.; X. Gonze *et al.Z. Kristallogr*., 2005, **220**, 558.

12 J. Tersoff and D. R. Hamann, *Phys. Rev. B*, 1985, **31**, 805.

13 O. Takeuchi, S. Yoshida, and H. Shigekawa, *Appl. Phys.Lett.*, 2004, **84**, 3645.

14 M. Godlewski and M. Kaminska, *J. Phys. C,* 1980, **13**, 6537.

15 R. K. Swank, *Phys. Rev*. 1967, **153**, 844.

16 D. Kitchen, A. Richardella,J.-M.Tang, M. E. Flatté and A. Yazdani, *Nature*, 2006, **442**, 436.

17 P. Mahadevan, A. Zunger, and D. D. Sarma, *Phys. Rev. Lett.* 2004, **93**, 177201.

18 D. Soundararajan, D. Mangalaraj, D. Nataraj, L. Dorosinskii, J. Santoyo-Salazar and M. J. Riley, *J. Magn. Magn. Mater.* 2009, **321**, 4108.

19 R. J. Meyer, C. B. Duke, A. Paton, E. So, J. L. Yeh, A. Kahn and P. Mark, *Phys. Rev. B*, 1980, **22**, 2875